A solar photothermo-catalytic combined process for the VOCs combustion and the subsequent CO_2 valorisation using noble metal-free catalysts

Roberto Fiorenza[a], Marianna Bellardita[b], Stefano Andrea Balsamo[a], Antonino Gulino[a], Marcello Condorelli[a], Giuseppe Compagnini[a], Salvatore Scirè[a] and Leonardo Palmisano[b]*

[a]*Dipartimento di Scienze Chimiche, Università di Catania, Viale A. Doria 6, 95125 Catania, Italy*

[b]*Dipartimento di Ingegneria, Università di Palermo, ed. 6, Viale delle Scienze, Palermo 90128, Italy*

***** Corresponding authors: *e-mail address*: rfiorenza@unict.it

Abstract

We here investigated a solar photothermo-catalytic combined process where the toluene (as volatile organic compound model) was first oxidized to CO_2 which was subsequently converted into solar fuels in a second reactor. For this aim two noble-metal free catalytic systems were used, namely MnO_x-ZrO_2, which gave the best results for the toluene removal, and brookite TiO_2-CeO_2 mixed oxides which were the most efficient in the subsequent CO_2 conversion. This latter reaction was further improved by the addition of small amounts of copper-based materials on brookite-ceria, acting as co-catalysts. The key point for both the examined reactions was the synergism between the thermocatalytic and the photocatalytic mechanisms that enhanced the energy saving and the catalytic performance. In particular, with the MnO_x-5wt%ZrO_2 catalyst 90% of toluene was converted into CO_2 at 180°C, about 50°C less than in the bare thermocatalytic tests and the obtained CO_2 was converted into CO (17.6 $\mu mol/g_{cat} \cdot h$) and CH_4 (7.9 $\mu mol/g_{cat} \cdot h$) with the CuO_x/TiO_2-3%wt CeO_2 sample at 120°C. The photothermo-catalytic activity was about 4 times higher than solar photocatalytic activity and greater than the thermocatalytic one that required a temperature above the 200°C. The proposed approach is promising to obtain solar fuels starting from toxic pollutants.

Keywords: VOCs removal, CO_2 conversion, photothermo-catalysis, noble metals-free catalysts, brookite, MnO_x.

1. Introduction

The removal of volatile organic compounds (VOCs) from outdoor and indoor environments is one of the current urgent tasks, especially considering the recent pandemic situation. Sustainable and green processes, such as heterogeneous photocatalysis, can provide performing solutions to improve air quality [1]. The complete mineralization of VOCs should be preferred in order to transform an air pollutant into less dangerous products as water and CO_2. However, the produced CO_2 is also an environmental issue, and today it must be considered as a resource to be exploited. Even if with the photocatalytic process it is possible to convert this gas in high added value products (i.e. solar fuels) with the fascinating processes of the artificial photosynthesis however, the process efficiency is often low [2].

In this contest, we originally proposed an integrated *VOCs-to solar fuels* approach, where the solar fuels were obtained starting from air pollutants mineralization. For this combined approach it is essential to ensure both the total VOCs combustion (i.e., without the formation of other by-products) and good yields to solar fuels. Recently, the application of hybrid catalysis, as the photothermo-catalysis, to both reactions (VOCs removal and CO_2 reduction) has allowed to achieve an energy saving compared to the thermocatalytic tests and to strongly enhance the performance compared to the photocatalytic route at room temperature [3–5].

In this work, we have explored and compared the photothermo-catalytic performance of noble metal-free mixed oxides in an integrated process where the toluene, chosen as VOC model, was first oxidized to CO_2, and this one was flowed in another reactor to be converted into solar fuels. This investigated multi-catalytic approach can help to design the optimal catalysts for both VOCs removal and CO_2 conversion. Furthermore, the optimization of the entire combined process allowed to propose, to the best of our knowledge for the first time, an efficient, environmentally friendly and economical strategy to remove dangerous contaminants from the air, reducing at the same time the consumption of energy, and obtaining chemicals with high added value.

To this end, the choice of suitable catalysts is essential. A photocatalytic semiconductor material displaying activity under solar radiation and redox thermocatalytic properties is required. The synthesis of mixed oxides/composites is the best and easiest way to

combine all of these characteristics. In this contest, the brookite TiO_2-CeO_2 composites showed promising performance in the photothermal approach for both VOCs removal and CO_2 reduction [3,4] due to the peculiar photoreduction properties of the brookite and the thermocatalytic redox properties of CeO_2.

Following this strategy, other transition metal oxides, such as MnO_x and ZrO_2, can be examined for their photocatalytic and redox properties by adopting this hybrid catalysis [6]. In this way it is possible to avoid the use of expensive and critical catalysts based on noble metals, widely applied for this type of reactions.

2. *Material and Methods*

2.1. Samples preparation

The MnO_x-ZrO_2 systems were synthesized by co-precipitation with NaOH (1 M) starting from the manganese (II) chloride tetrahydrate and the zirconyl nitrate hydrate. The powders were dried at 120°C and calcined in air at 600°C for 2 h. The catalysts were coded as MnZrX where X is the wt % of ZrO_2.

The brookite TiO_2-CeO_2 samples were prepared through the wetness impregnation following the same procedures reported in the ref [4]. The code used for this samples is TiCeX where X is the wt % of CeO_2.

Furthermore, we have investigated the influence of the addition of small amounts of copper-based co-catalysts on the brookite TiO_2-CeO_2. In particular, CuO (0.5 wt%) was impregnated by the wetness method on the as-prepared brookite TiO_2-CeO_2 using $Cu(NO_3)_2 \cdot 2.5H_2O$ as the precursor. The obtained sample were dried overnight at 120°C and calcined at 300°C for 2h.

Cu_2O (0.5 wt%) was instead deposited on brookite TiO_2-CeO_2 by chemical reduction of $CuCl_2$. The stoichiometric amount of $CuCl_2$ was previously dissolved in a solution of NaOH (2 M) and stirred for 30 min. Afterwards a fixed amount of $NaBH_4$ ($NaBH_4$/$CuCl_2$ molar ratio of 2:1) was added dropwise and stirred for other 30 min. The obtained slurry was centrifuged at 8000 rpm for 10 min and washed with deionized water several times. Finally, the powders were dried under vacuum at 55°C for 6 h.

We have also synthesized a bimetallic oxides-based sample i.e., the CuO (0.3 wt%)-Cu_2O (0.3 wt%)/brookite TiO_2-3 wt%CeO_2 depositing the Cu_2O on the as-prepared

CuO/brookite TiO_2-3 wt%CeO_2 with the same procedures previously discussed. This sample was named as CuO_x/TiCe3.

2.2. Samples characterization

The samples were structurally (XRD, Raman and FTIR spectroscopies), texturally (N_2 adsorption-desorption measurements), morphologically (SEM and TEM), optically (UV-vis DRS and PL) and superficially (XPS) characterized. The details of the measurements are reported in the supporting information.

2.3. Catalytic activity experiments

The photothermo-catalytic process was employed using two photoreactors. The first one, used for the toluene photothermo-catalytic oxidation in the gas phase at atmospheric pressure, was a quartz flow reactor utilizing the reaction conditions reported in the supporting information. The obtained CO_2 was continuously flowed in a second quartz reactor and mixed with water vapour until the saturation of the catalysts surface. Successively, the reactor was closed, heated at 120°C and irradiated for 5 h. The products were analysed by GC. Two identical solar lamps (Osram Ultra Vitalux 300W; 10.7 mW/cm^2) were used for both the reactions. The scheme of the integrated process (Fig. S1) and the details of the experimental set-up are further discussed in the supporting information.

3. Results and discussion

3.1 First reactor: Solar photo-assisted thermocatalytic oxidation of toluene to CO_2

In order to obtain an integrated approach able to produce solar fuels starting from air contaminants, we chose the toluene as model VOC, and on the basis of the definitions of *Ma et al.* [7], we performed the reaction in the solar photo-assisted thermocatalysis. In this way, in our experimental conditions, the thermocatalytic mechanism and the heating power ensured the total combustion of toluene, thus avoiding the formation of other compounds that can poison the catalyst placed in the second consecutive photoreactor (see fig. S1). Furthermore, the contextual solar irradiation made it possible to decrease the conversion temperature of the toluene with respect to the bare thermocatalytic tests. Indeed, from the Fig. 1A it is possible to note as the MnZr5 sample reached the toluene

T90 (temperature at which the 90% of toluene was converted into CO_2) at a relative low temperature (180°C) decreasing of about 50°C the T90 of the bare thermocatalytic tests [6]. We have compared the single oxides and the best composites (MnZr5 and TiCe3) that showed the best performance in the toluene photothermo-catalytic oxidation. The influence of the amount of zirconia on MnO_x and of ceria on brookite TiO_2 was previously investigated [4,6]. The order of activity was MnZr5 > Mn_3O_4 ≥ TiCe3 ≥ZrO_2 > brookite TiO_2 > CeO_2. This highlighted as the composites exhibited higher performance compared to the bare oxides and how the synergism between the manganese oxide and the zirconia was more performing for this reaction compared to the TiO_2-CeO_2 sample. Indeed, although both the mixed oxides showed a similar optical bandgap (3.2-3.3 eV, Table S1) the higher surface area of MnZr5 (85 m^2/g) compared to TiCe3 (68 m^2/g), coupled with the peculiar surface and chemical features, were determining to increase the toluene conversion (Table S1). The driven force of the reaction was the thermocatalytic mechanism through a Mars-Van Krevelen (MvK) pathway [8], where the oxygens in the gas-phase and the surface and lattice oxygens of reducible catalysts contributed to the total oxidation reaction. The high surface area of MnZr5, the higher reducibility/mobility of its surface oxygen and its higher thermocatalytic activity compared to TiCe3 explained the different catalytic behaviour. In this photo-assisted thermocatalytic approach, the solar photocatalysis helped to decrease the toluene T90 with the formation of hydroxyl and superoxide radicals, that being more reactive of the oxygens in the gas-phase, further promoted the MvK mechanism, also boosted up by the redox properties of MnO_x. The H_2-TPR profiles of the analysed samples confirm these features (Fig. 1B). The bare brookite did not show reduction peaks, as expected considering that the reduction of TiO_2 started at temperature higher of 500°C, as the bare zirconia [9]. The bare CeO_2 exhibited a reduction feature at about 500°C attributed to the start of the surface ceria oxygen reduction that ends at higher temperatures [10]. Due to the low amount of ceria on TiO_2 the profile of TiCe3 is similar to the unmodified brookite. The bare Mn_3O_4 exhibited a broad peak centred at 361°C, assigned to the $Mn_3O_4 \rightarrow MnO$ reduction [11]. In the MnZr5 profile a low temperature reduction peak (207°C) is present and it can be assigned to the $Mn_2O_3 \rightarrow Mn_3O_4$ reduction [11]. The formation of Mn_2O_3 in the MnZr5 sample, favoured by the small amount of zirconia [6], was also confirmed by XRD (Fig. S2). The lower reduction peak of this sample is related to the very high mobility of oxygen, beneficial

for the solar assisted MvK mechanism, and may explain the greater activity of this catalyst in the combustion of toluene compared to other materials. Another evidence that correlates the reduction properties of the MnZr5 with its photothermo activity is the similar values of the initial TPR reduction temperature and the low reduction temperature peak (about 154°C and 200°C respectively) with the measured toluene T90 (180°C) (Fig. 1B). The morphology of MnZr5, determined by SEM (Fig.S2), was characterized by nearly spherical particles.

3.2 Second reactor: Solar photo-thermo co-catalytic CO_2 conversion

To evaluate the conversion of the CO_2 produced in the first reactor from the photo-assisted thermocatalytic oxidation of toluene in the presence of MnZr5 catalyst, it was mixed with water vapor and flowed in a second batch reactor (Fig. S1).

The results of the CO_2 conversion at 120 °C are illustrated in the Fig. 2. In this case, a photo-thermal co-catalysis with the synergism between the two mechanisms is necessary to guarantee a good production of solar fuels (as definition, the activity of the combined approach should be higher than the sum of the single thermocatalysis and photocatalysis [7]). The CuO_x/TiCe3 system resulted the best sample and the formation rate for CO and CH_4 at 120°C was about 3.5 times and 5 times, respectively, higher compared to solar photocatalytic tests (at 30°C), whereas for the thermocatalytic conversion it was required a temperature higher than 180°C (instead of the 120°C of the photo-thermo co-catalysis) with, however, lower performance up to 300°C (Table S2). In this case, being the CO_2 activation a more difficult reaction than the photothermal oxidation of toluene, only the brookite TiO_2-based samples were able to convert the CO_2 into solar fuels, due to more suitable band positions of TiO_2 and to the strong synergism between the brookite and ceria to activate the CO_2 [3]. Moreover, in accordance with the literature [12] the presence of co-catalysts is needed to improve the synchronous reaction between the excited electrons, the protons arising from the water oxidation by the holes, and the CO_2 adsorbed on the surface of the samples. Due to the peculiar band positions, the copper oxides are particularly suitable for the CO_2 reduction, as well as the metallic copper [13]. The CO and the CH_4 formation increased of about 8 and 9 times respectively, comparing the Cu_2O/TiCe3 sample with the TiCe3 (Fig. 2), with a CO_2 conversion that enhanced from the 24% of the TiCe3 to the 52% of the Cu_2O/TiCe3. A further increase above all in the

formation of methane was obtained with the bimetallic oxide co-catalyst (CuO_x/TiCe3), which duplicated the evolution of CH_4 with respect to Cu_2O/TiCe3 (conversion of CO_2 by 61%).

The different catalytic behaviour of the samples can be correlated to the modification of the structural, surface and optical properties of the TiCe3 composite due to the addition of the Cu-based co-catalysts. The Raman and XRD analyses (Figs. S3) pointed to the presence of the only brookite crystalline phase in the as-synthesized samples as indicated by the typical Raman vibrational modes of this phase, with the main one at 155 cm^{-1} and to the contextual absence of the fingerprints vibration at 516 cm^{-1} and 446 cm^{-1} characteristic of the anatase and rutile phases, respectively (Fig. S3A) [14]. Also the main XRD peak at $2\theta = 30.8°$ (Fig. S3B) was another hint of the pure brookite phase [14]. The absence of XRD signals related to copper oxides and CeO_2 was reasonably due to the low amount/good dispersion of these species on the brookite TiO_2. On the contrary, in the CuO_x/TiCe3 sample it is possible to see two weak Raman bands at 581 cm^{-1} and 1067 cm^{-1} related to the Cu_2O and CuO respectively (Fig. S3A) [15,16]. Also in this case, the samples showed a spherical morphology (inset Fig. S3B), whereas the addition of the copper-based co-catalysts led to a slight increase of the BET surface area in the CuO_x/TiCe3 sample (74 m^2/g) compared to the TiCe3 sample (68 m^2/g). However, these values were lower respect to the pure brookite (80 m^2/g, Table S1) probably due to the further thermal treatments used for the preparation of the TiCe3-based samples.

The Fig. S4A showed the XPS spectra of the examined samples, in the Ti region. For all the samples, the Ti $2p_{3/2,\ 1/2}$ spin-orbit components lie at 458.4 and 464.1 eV, respectively, and these energies are almost coincident with those observed for the pure brookite phase [4,17]. Three signals in the O 1s region, present in all the samples, at 529.6, 531.3 and 535.7 eV (Table 1) mainly refer to the Ti-O, Ti-OH and Ti-H_2O states. In the Ce 3d region, nevertheless the low intensity signals and the low concentration, it was possible to spot for all the samples five different components at 881.4, 884.8, 899.4, 903.5 and 915.4 eV, typical of the overlap of Ce^{4+} and Ce^{3+} states [18,19] (Table 1). In the Cu 2p region (Fig. S4B, Table 1) it is possible to note for the CuO/TiCe3 the signals at 933.9 and 953.8 eV with a 19.9 eV spin–orbit separation, consistent with the Cu^{2+} states [20], whereas for the Cu_2O/TiCe3 the two peaks at 932.1 and 951.7 eV were related to the presence of Cu^+ [21]. As reported in the literature for similar samples, it is not possible

to exclude the contemporaneous presence of metallic copper species in the Cu_2O/TiCe3 and CuO_x/TiCe3 samples being both the XPS binding energies and spectral shape identical for Cu^0 and Cu^+ (as Cu_2O)[22,23]. In theory it could be possible to discriminate between the Cu^+ and the Cu^0 species by observing the energies of their LMM-2 Auger lines but this observation was not possible because of the very low intensity related to the Auger signals as a consequence of the low amount of the co-catalysts on the TiO_2. In the CuO_x/TiCe3 sample the two Cu 2p peaks are at about 0.5 eV higher binding energy (B.E.) with respect to those observed for the Cu_2O/TiCe3 (Fig. S4B, Table 1) and this is correlated to the occurrence of a partial oxidation of copper due to the contemporaneous presence of the Cu^{2+} species.

On the basis of the catalytic results, on the best samples (Cu_2O/TiCe3 and CuO_x/TiCe3) we have evaluated the possible surface properties variations due to the CO_2 reduction reaction, comparing the XPS spectra of the fresh and the used samples. Interestingly, in the Ti region (Table 1) the used CuO_x/TiCe3 sample showed the Ti $2p_{3/2, 1/2}$ signals at about 0.4 eV higher B.E. with respect to those observed on the fresh sample. This can be due to some CO coordinated to Ti(IV) ions, arising from the formation of some reaction intermediates, that on the contrary were totally desorbed from the surface of the Cu_2O/TiCe3, the Ti 2p signals of this sample before and after the reaction being highly similar. The main variation related to Ce were found in the surface concentration. For the used Cu_2O/TiCe3, the experimental Ce/Ti at% was 1.5, close to the nominal value (1.4 at%), whereas it was 4.0 in the fresh sample, thus indicating some cerium bulk segregation occurring during the catalytic reaction (Table S3). Also with the CuO_x/TiCe3 a slight segregation of cerium in the bulk was detected after the CO_2 conversion (Ce/Ti at% 2.7 for the fresh sample, decreased to 2.3 after use, Table S3). Contextually, it was detected an increased copper surface enrichment after the reaction and especially with CuO_x/TiCe3. The Cu/Ti at% ratio, indeed, rose from 2.7 of the fresh sample to 11.2 after the reaction, much higher than the nominal ratio (0.7). With the Cu_2O/TiCe3 this surface segregation was less evident but however present, the Cu/Ti at% of the used sample being 1.25 times higher compared to the fresh one (Table S3). No substantial variations were detected after the catalytic tests in the signals of the Cu 2p region (Table 1).

The optical properties of the TiCe-based samples determined by the UV-DRS and PL spectroscopies are illustrated in the Figs. S5 and the estimated values of the optical

bandgap are reported in the Table S1. A little red-shift in the UV-DRS spectra (Fig. S5A) was verified with the addition of cuprous oxide and of the bimetallic species CuO_x on TiCe3, that pointed to a small decrease of the bandgap compared to the unmodified TiCe3 (Table 1). Furthermore, a feature at about 660-700 nm, assigned to the interfacial charge transfer from the valence band of TiO_2 to the Cu_2O/CuO_x [24], is present in these samples. The PL spectrum of TiCe3 showed several bands attributed to band-to band emission of brookite (at about 390 nm), to the presence of self-excited excitons (at 411 nm) and to the oxygen vacancies induced by CeO_2 (band at 464 nm) [3,4] (Fig. S5B). The addition of the copper oxides co-catalysts quenched these bands with the formation of others at 432, 485 and 540 nm. The first one is attributed to the formation of defect states, surface oxygen vacancies and/or to the excitons recombination via bulk defects, the second one is ascribed to the excitonic transitions from sublevels of the conduction band, generated by the presence of the copper species, to the valence band of TiCe3. The last one was probably due to the formation of surface defects in the crystalline structure of TiCe3 [25]. The intensity of these bands was lower in the Cu_2O/TiCe3 and CuO_x/TiCe3 samples pointing to an increased charge carrier separation in these materials [26].

The increased charge carrier separation, the presence of the brookite phase and an important surface segregation phenomenon, especially evinced with the CuO_x/TiCe3 sample (the best one for the CO_2 conversion) were the key features that allowed to boost up the solar fuels formation from the CO_2 arising from the first reactor.

3.3 Photo-thermal co-catalysis mechanism of the CO_2 conversion

The proposed reaction mechanism for the CO_2 reduction, coming from the solar assisted photothermo catalytic oxidation of toluene, was depicted in the Fig. 3. Different processes synergistically act to obtain the solar fuels using the best catalyst (CuO_x/TiCe3) for this second reaction: (i) an efficient charge carriers separation, established thanks to the heterojunction between the brookite and CeO_2 [3,4,27] and to the presence of the copper-based co-catalysts as determined by the PL measurements; (ii) the synergism between the thermocatalytic and the photocatalytic mechanism. This allowed to improve the proton mobility generated from the oxidation of water (i.e. the rate determining step of the CO_2 photoreduction [3,28]), ensuring the synchronous reaction among the excited

electrons, the protons and the adsorbed CO_2. Indeed, comparing the apparent activation energy (E_a) of the thermocatalytic and of the photo-thermal co-catalytic tests using the CuO_x/TiCe3 sample (Fig. S6) it is possible to note as with the hybrid catalysis the E_a was strongly reduced (for the CO formation from 41.2 kJ/mol of the thermocatalytic tests to 9.6 kJ/mol of the photo-thermo co-catalysis and for the CH_4 formation from 33.5 kJ/mol to 10.2 kJ/mol) pointing to as the multi catalytic approach is essential to improve the solar fuels formation; (iii) the high surface enrichment of the copper-based species on CuO_x/TiCe3, as detected by XPS. Indeed, all the Cu species are beneficial for the CO_2 photothermo reduction, the cuprous oxide acts as electrons mediator due to its high energetic conduction band (CB) (-1.27 eV) [29], the cupric oxide favours the CO_2 adsorption due to its basic sites [30], whereas the metallic copper facilitates the electron mobility decreasing in this way the kinetic barriers for the CO_2 reduction [13]. For these reasons, in the sample where all of these species are present (i.e., the CuO_x/TiCe3 as established by XPS) the solar fuels formation was strongly increased. Moreover, the XPS after the tests stated the possible formation of intermediate species on CuO_x/TiCe3 with a further copper-based species surface enrichment. In the Figs. S7 are reported the FTIR spectra performed before and after the reduction of CO_2. As confirmation of the previous observations, the fresh CuO/TiCe3 sample showed a band at 1384 cm^{-1} associated to the monodentate carbonate [31] formed after the reaction of the atmospheric CO_2 with the basic surface sites of the CuO [30]. In the used samples no substantial variations were detected pointing to the desorption of intermediate products, whereas the spectra of the used CuO_x/TiCe3 was completely different (Figs. S7). In this sample both monodentate (bands at 1463 cm^{-1} and at 1332 cm^{-1}) and bidentate (1261 cm^{-1} and 995 cm^{-1}) carbonates together to other bands at lower wavenumber, associated to the interaction of the copper species with the CO_2, were present [32]. The formation of these intermediates can favour the formation of methane, being these compounds holes scavengers, further increasing the availability of the excited electrons (the CH_4 formation requires 8 electrons and 8 protons) and facilitating the CO_2 and the carbonates reduction [33]. Indeed, with the CuO_x/TiCe3 it was measured the highest CH_4 evolution (Fig. 2). These reactions were favoured on this latter catalyst by the solar photo-thermo-co catalysis that enriched the surface of TiCe3 of the copper species; (iv) finally, a good catalytic stability (Fig. S8) was verified after four consecutive runs on CuO_x/TiCe3 powders. This is another

promising point being the photocorrosion one of the main problems of the copper-based catalysts (especially based on cuprous oxide [13,29]). From the mechanism proposed in the Fig. 3, considering the reported values of the bands positions [13, 27, 29] and the literature concerning similar systems [29, 34, 35] it is reasonable that, due to the high negative potential of the CB of the copper-based co-catalyst, the excited electrons arising from the TiCe heterojunction can recombine with the holes of the CuO_x system. In this case, this phenomenon, being limited due to the very low amount of the copper species, can be regarded as a positive aspect decreasing the copper photocorrosion [29] caused by the migration of the holes in the valence band of the CuO_x (Fig. 3). Additionally, it causes the generation of heat that can further favour the solar photo-thermo-co catalysis, and allows to fully exploit the high reduction potential of the excited electrons of the Cu-based co-catalysts, boosting up the CO_2 reduction.

4. Conclusions

The high versatility of the proposed hybrid catalytic approach allowed to convert a toxic pollutant as the toluene to CO_2 and subsequently to transform it into solar fuels.
The photo-assisted thermocatalytic approach allowed to totally mineralize the toluene into CO_2 with the MnO_x-ZrO_2 catalyst at relative low temperature (180°C) and the obtained greenhouse gas was further converted into CO and CH_4 using the CuO_x/TiO_2-CeO_2 sample. For the toluene removal the solar-assisted Mars Van Kreveln mechanism boosted up by the redox properties of the manganese oxide allowed to decrease of 50°C the temperature necessary for the 90% of conversion of toluene compared to the bare thermocatalytic tests. The CuO_x/TiO_2-CeO_2 system permitted to increase the formation of solar fuels from the previously evolved CO_2 thanks to the different synergisms of the solar photo-thermal co-catalytic mechanism. This circular fascinating strategy is, at the best of our knowledge, not yet explored and it is encouraging to propose new and sustainable ways to obtain high added value products starting from air contaminants and using not-critical and noble metals-free catalysts.

Acknowledgments

We thank the PIACERI 2020-2022 project of the University of Catania, the BRIT for the Raman and XPS facilities and the Institute of Nanochemistry of the University of Cordoba (Spain) for the TEM measurements.

References

[1] S. Kim, S. Kim, H.-J. Park, S. Park, J.Y. Kim, Y.W. Jeong, H.H. Yang, Y. Choi, M. Yeom, D. Song, C. Lee, Environ. Res. 204 (2022) 112036.

[2] W. Zhang, A.R. Mohamed, W. Ong, Angew. Chemie Int. Ed. 59 (2020) 22894–22915.

[3] R. Fiorenza, M. Bellardita, S.A. Balsamo, L. Spitaleri, A. Gulino, M. Condorelli, L. D'Urso, S. Scirè, L. Palmisano, Chem. Eng. J. 428 (2022).

[4] M. Bellardita, R. Fiorenza, L. D'Urso, L. Spitaleri, A. Gulino, G. Compagnini, S. Scirè, L. Palmisano, Catalysts 10 (2020) 765.

[5] N. Keller, J. Ivanez, J. Highfield, A.M. Ruppert, Appl. Catal. B Environ. 296 (2021) 120320.

[6] R. Fiorenza, R.A. Farina, E.M. Malannata, F. Lo Presti, S.A. Balsamo, Catalysts. 12 (2022) 85.

[7] R. Ma, J. Sun, D.H. Li, J.J. Wei, Int. J. Hydrogen Energy. 45 (2020) 30288–30324.

[8] J.-J. Li, E.-Q. Yu, S.-C. Cai, X. Chen, J. Chen, H.-P. Jia, Y.-J. Xu, Appl. Catal. B Environ. 240 (2019) 141–152.

[9] M. Jabłońska, Catal. Commun. 70 (2015) 66–71.

[10] A. Trovarelli, G. Dolcetti, C. de Leitenburg, J. Kašpar, P. Finetti, A. Santoni, J. Chem. Soc., Faraday Trans. 88 (1992) 1311–1319.

[11] E.R. Stobbe, B.A. de Boer, J.W. Geus, Catal. Today. 47 (1999) 161–167.

[12] S. Al Jitan, G. Palmisano, C. Garlisi, Catalysts. 10 (2020) 227.

[13] H. Xie, J. Wang, K. Ithisuphalap, G. Wu, Q. Li, J. Energy Chem. 26 (2017) 1039–1049.

[14] M. Bellardita, A. Di Paola, B. Megna, L. Palmisano, Appl. Catal. B Environ. 201 (2017) 150–158.

[15] Y. Liu, F. Ren, S. Shen, Y. Fu, C. Chen, C. Liu, Z. Xing, D. Liu, X. Xiao, W. Wu, X. Zheng, Y. Liu, C. Jiang, Appl. Phys. Lett. 106 (2015) 123901.

[16] A. Mehta, R.A. Rather, B. Belec, S. Gardonio, M. Fang, M. Valant, Energies. 15 (2022) 1–16.

[17] X. Gao, Y. Jiang, Y. Zhong, Z. Luo, K. Cen, J. Hazard. Mater. 174 (2010) 734–739.

[18] E. Bêche, P. Charvin, D. Perarnau, S. Abanades, G. Flamant, Surf. Interface Anal. 40 (2008) 264–267.

[19] L. Qiu, F. Liu, L. Zhao, Y. Ma, J. Yao, Appl. Surf. Sci. 252 (2006) 4931–4935.

[20] F. Lupo, S. Gentile, F.P. Ballistreri, G.A. Tomaselli, M.E. Fragalà, A. Gulino, Analyst. 135 (2010) 2273.

[21] S. Poulston, P.M. Parlett, P. Stone, M. Bowker, Surf. Interface Anal. 24 (1996) 811–820.

[22] Y. Zheng, L. Zhang, J. Guan, S. Qian, Z. Zhang, C.K. Ngaw, S. Wan, S. Wang, J. Lin, Y. Wang, ACS Sustain. Chem. Eng. 9 (2021) 1754–1761.

[23] N. Pauly, S. Tougaard, Surf. Sci. 641 (2015) 326–329.

[24] K. Wang, Z. Bielan, M. Endo-Kimura, M. Janczarek, D. Zhang, D. Kowalski, A. Zielińska-Jurek, A. Markowska-Szczupak, B. Ohtani, E. Kowalska, J. Mater. Chem. A. 9 (2021) 10135–10145.

[25] K. Sabzehei, S.H. Hadavi, M.G. Bajestani, S. Sheibani, Solid State Sci. 107 (2020) 106362.

[26] J. Liqiang, Q. Yichun, W. Baiqi, L. Shudan, J. Baojiang, Y. Libin, F. Wei, F. Honggang, S. Jiazhong, Sol. Energy Mater. Sol. Cells. 90 (2006) 1773–1787.

[27] J. Zhao, Y. Wang, Y. Li, X. Yue, C. Catal. Sci. Technol. 6 (2016) 7967–7975.

[28] S. Fang, Y.H. Hu, Chem. Soc. Rev. (2022) 3609–3647.

[29] S. Ali, J. Lee, H. Kim, Y. Hwang, A. Razzaq, J.W. Jung, C.H. Cho, S. Il In, Appl. Catal. B Environ. 279 (2020) 119344.

[30] M.A. Ávila-López, E. Luévano-Hipólito, L.M. Torres-Martínez, J. Photochem. Photobiol. A Chem. 382 (2019) 111933.

[31] A. Davydov, Molecular spectroscopy of oxide catalyst surfaces, John Wiley &Sons,Inc.: Hoboken, NJ. 2003.

[32] S. Chen, T. Cao, Y. Gao, D. Li, F. Xiong, W. Huang, J. Phys. Chem. C. 120 (2016) 21472–21485.

[33] N.M. Dimitrijevic, B.K. Vijayan, O.G. Poluektov, T. Rajh, K.A. Gray, H. He, P. Zapol, J. Am. Chem. Soc. 133 (2011) 3964–3971.

[34] L.I. Ibarra-Rodriguez, J.C. Pantoja-Espinoza, E. Luévano-Hipólito, L.F. Garay-Rodríguez, A. López-Ortiz, L.M. Torres-Martínez, V.H. Collins-Martínez, J. Photochem. Photobiol. 11 (2022) 100125.

[35] P.K. Prajapati, D. Garg, A. Malik, D. Kumar, V. Amoli, S.L. Jain, J. Environ. Chem. Eng. 10 (2022) 108147.

Table 1 XPS Binding Energies (eV) of the analysed samples

Samples	**Ti 2p**	**O 1s**	**Ce 3d**	**Cu 2p**
Brookite TiO_2	458.5 464.1	529.7 531.1 535.5	/	/
TiCe3	458.4 464.1	529.4 531.2 535.6	881.2 884.8 899.4 903.5 915.6 (Ce^{4+})	/
CuO/TiCe3	458.3 464.1	529.5 531.4 535.6	881.3 884.8 899.4 903.5 915.5 (Ce^{4+})	933.9 953.8
Cu_2O/TiCe3	458.4 464.1	529.6 531.3 535.7	881.4 884.8 899.4 903.5 915.4 (Ce^{4+})	932.1 951.7
Cu_2O/TiCe3 after test	458.5 464.0	530.1 Broad tail 535.0	881.2 884.8 899.4 903.3 915.4 (Ce^{4+})	932.0 951.9
CuO_x/TiCe3	458.5 464.2	529.8 531.7 535.9	881.7 884.8 899.3 903.3 915.6 (Ce^{4+})	932.6 952.2
CuO_x/TiCe3 after test	458.9 464.6	529.8 531.7 535.9	881.5 885.0 899.9 903.2 915.7 (Ce^{4+})	932.1 952.0

Captions to figures

Fig. 1 (A) Solar photo-assisted thermocatalytic oxidation of toluene and, (B) H_2-TPR profiles of the examined samples.

Fig. 2 Solar photo-thermo co-catalytic CO_2 reduction (T= 120°C) on the examined catalysts. They were irradiated for 5 h.

Fig. 3 Proposed mechanism for the CO_2 conversion arising from the toluene photo-thermocatalytic oxidation.

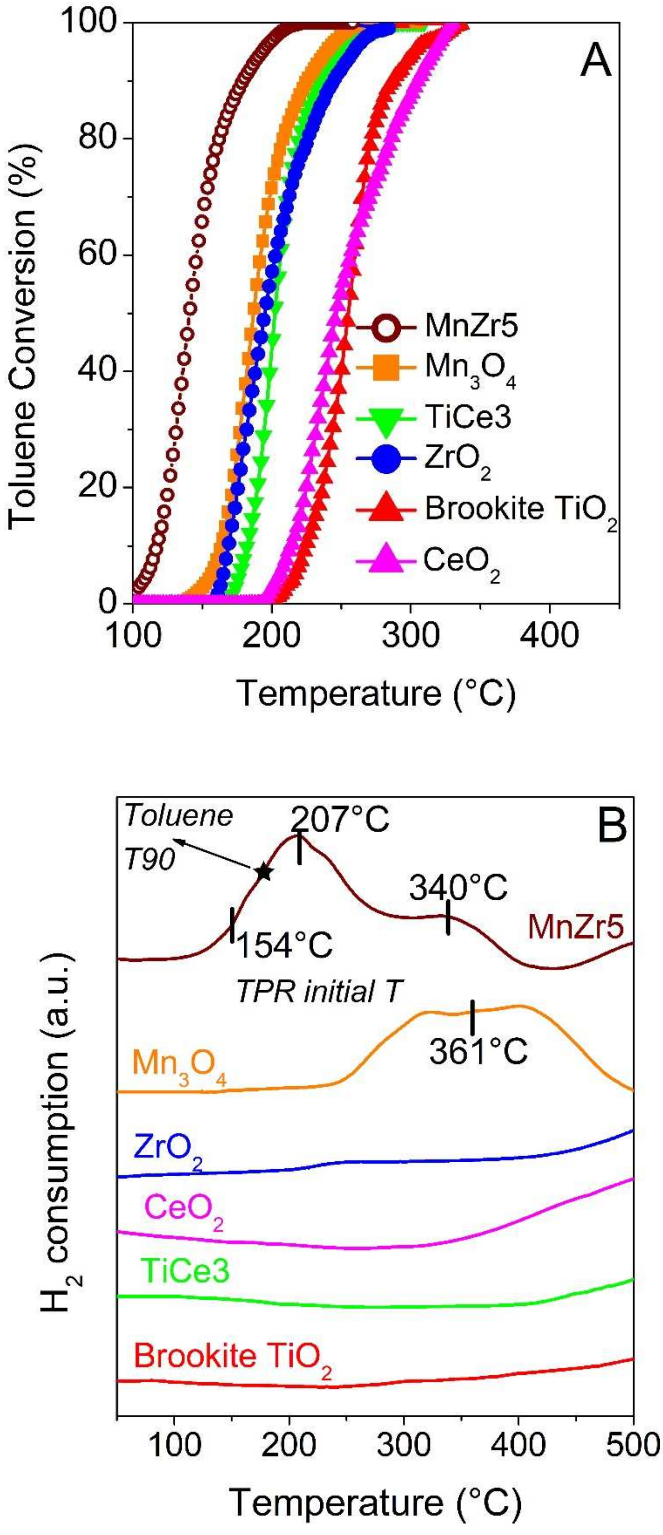
A
Toluene Conversion (%)
Temperature (°C)
MnZr5
Mn3O4
TiCe3
ZrO2
Brookite TiO2
CeO2
B
Toluene
T90
207°C
340°C
154°C
MnZr5
TPR initial T
361°C
Mn3O4
ZrO2
CeO2
TiCe3
Brookite TiO2
H2 consumption (a.u.)
Temperature (°C)

Fig. 1

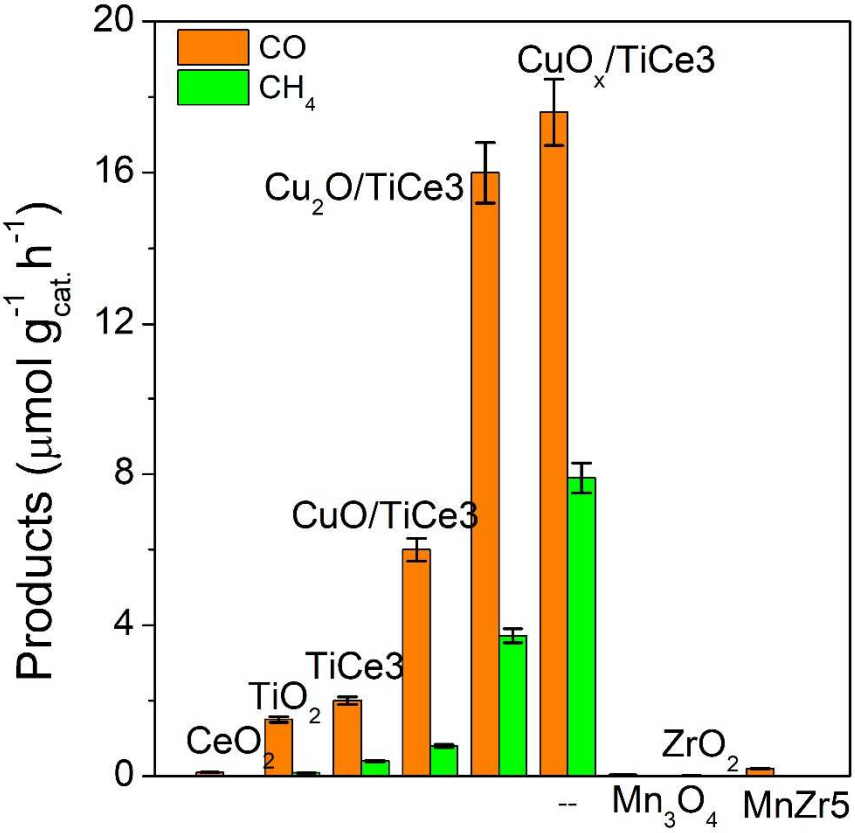
20
16
12
8
4
0
Products (μmol g$_{cat.}^{-1}$ h^{-1})
CO
CH$_4$
CeO$_2$
TiO$_2$
TiCe3
CuO/TiCe3
Cu$_2$O/TiCe3
CuO$_x$/TiCe3
ZrO$_2$
--
Mn$_3$O$_4$
MnZr5

Fig. 2

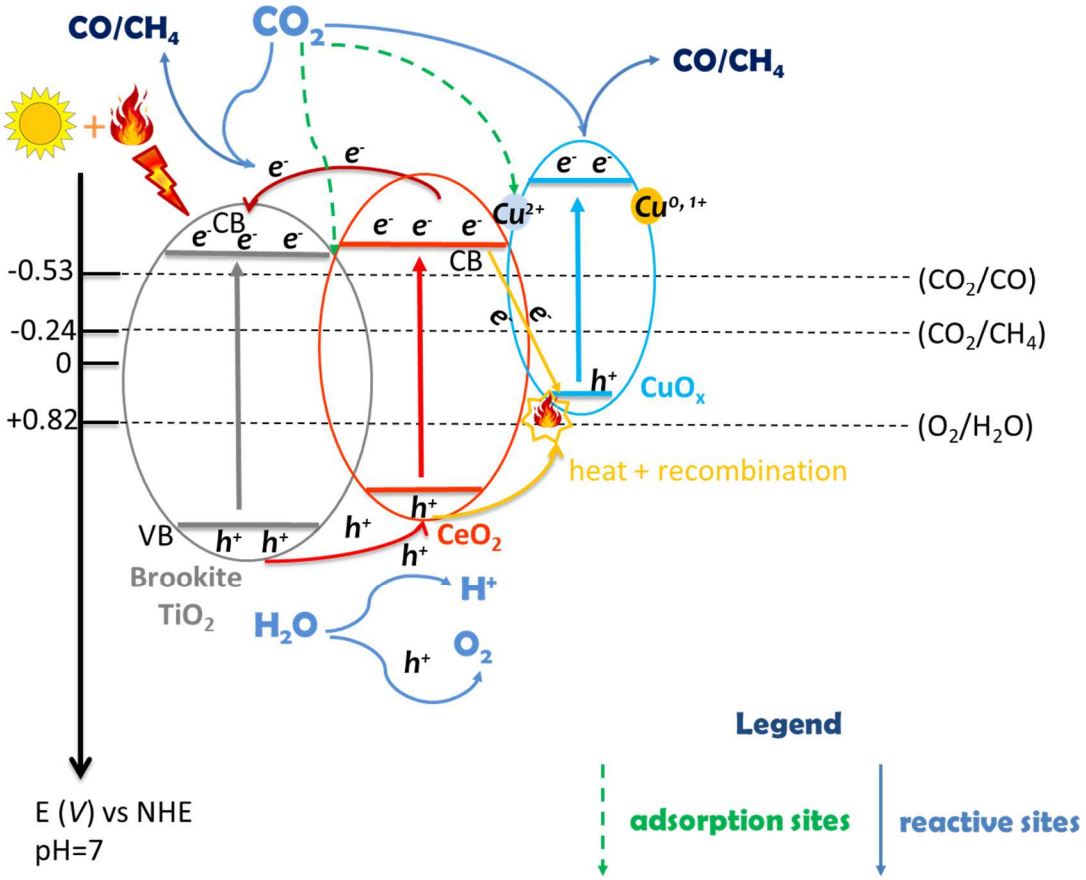
CO/CH4
CO2
CO/CH4
e-
CB
Cu2+
Cu0, 1+
-0.53
-0.24
0
+0.82
(CO2/CO)
(CO2/CH4)
(O2/H2O)
h+
CuOx
heat + recombination
VB
Brookite
TiO2
CeO2
H2O
H+
O2
E (V) vs NHE
pH=7
Legend
adsorption sites
reactive sites

Fig. 3

A solar photothermo-catalytic combined process for the VOCs combustion and the subsequent CO_2 valorisation using noble metal-free catalysts

Roberto Fiorenza[a], Marianna Bellardita[b], Stefano Andrea Balsamo[a], Antonino Gulino[a], Marcello Condorelli[a], Giuseppe Compagnini[a], Salvatore Scirè[a] and Leonardo Palmisano[b]*

[a]*Dipartimento di Scienze Chimiche, Università di Catania, Viale A. Doria 6, 95125 Catania, Italy*

[b]*Dipartimento di Ingegneria, Università di Palermo, ed. 6, Viale delle Scienze, Palermo 90128, Italy*

***** Corresponding authors: *e-mail address*: rfiorenza@unict.it

Supporting information

- **Samples Characterization**

X-ray powder diffraction (XRD) measurements were carried out with a PANalytical X'pertPro X-ray diffractometer using a Cu K_α radiation. Diffraction peaks of crystalline phases were compared with those of standard compounds present in the JCPDS Data File.

The Raman spectra were performed by using the second harmonic (532 nm) of an Nd:YAG laser in the backscattering mode using a Witec Alpha 300 RS instrument. For all the samples, the power of the exciting laser was 5 mW and the acquisition time and accumulation number were fixed respectively at 10 seconds and 10 spectra. The Raman intensity map was acquired with the same apparatus but with 10 mW of power and an accumulation time of 0.1 seconds.

FTIR measurements were carried out with a Spectrum Two System (Perkin Elmer), using KBr powders as reference.

The N_2 adsorption-desorption determinations were performed with a Thermo Quest (Sorptomatic 1990) apparatus. The powders were pre-treated by outgassing for 24 h at 50°C.

The SEM morphology of the examined samples was obtained with a ZEISS SUPRA 55 VP equipped with an energy dispersive X-ray (EDX) INCA-Oxford windowless detector.

The TEM images were carried out with a JEOL JEM 1400 microscope. The samples were dispersed in 2-propanol and sonicated for 30 min. Afterwards they were deposited onto copper grids.

The UV-Vis DRS (Diffuse Reflectance Spectroscopy) was performed with a spectrometer JASCO V-670. The E_g (optical band gap) of the samples was estimated plotting the modified Kubelka–Munk function versus the hν.

The photoluminescence (PL) spectra were determined using a JobinYvon instrument (Horiba) and an excitation λ of 300 nm.

X-ray photoelectron spectra (XPS) were measured at 45° take-off angle relative to the surface plane with a PHI 5000 VersaProbe Multi Technique System (Physical Electronics GmbH, Feldkirchen, Germany, base pressure of the main chamber 2.0×10^{-8} Pa). Samples were excited with monochromated Al Kα X-ray radiation using a pass energy of 11.75 eV. Because of some very low intensity signals (Cu and Ce) the XP spectra were accumulated for about 24 h for each sample. The XPS peak intensities were obtained after a Shirley background removal [1,2]. The instrumental energy resolution was ≤ 0.4 eV. Spectra calibration was achieved by fixing the main C 1s signal at 285.0 eV. The atomic concentration analysis was performed by taking into account the relevant atomic sensitivity factors. Note that, the nominal 3 weight % of CeO_2 in TiO_2 corresponds to a 1.4 mol % of CeO_2 in TiO_2 for all samples. In addition, the nominal 0.5 weight % of Cu_2O in TiO_2 corresponds to 0.58 mol % as well of CuO in TiO_2. Moreover, the nominal 0.3 weight % of Cu_2O plus 0.3 weight % of CuO in TiO_2 correspond to 0.66 mol %.

The H_2-TPR (Temperature programmed reduction) measurements were carried out in a conventional flow apparatus with a TCD detector, using at heating rate of 10°C/ min and a gas mixture of 5 vol% H_2 in Ar.

- **Experimental set-up for the solar photothermo-catalytic tests**

In the figure S1 the used experimental set-up is illustrated. In particular, in the first reactor (5) the toluene photothermo-catalytic oxidation was carried out. The reaction was performed continuously in a flow reactor packed with the powder sample (P = 1 atm, 150 mg, 80–140 mesh). For each test, the reactor was heated with a small programable oven and irradiated from the top by a solar lamp (6) (OSRAM Vitalux 300 W, 10.7 mW/cm^2). The reactant mixture was adsorbed–desorbed over the catalyst (0.1 vol.% VOCs; 10 vol.% air, rest He) for 30 min to assure the steady-state. By using the above procedure, conversion and selectivity were within 3–5% of reproducibility. Preliminary runs performed at different flow rates showed the absence of external diffusional limitations. The absence of internal diffusion limitations was verified by running experiments with different grain size powders. We excluded the occurrence of heat transfer limitations because we found that the temperature of the reactor at different heights was substantially the same, reasonably due to the low

concentration of the reactants used in the catalytic tests. The reactant mixture was fed to the reactor by flowing a part of the He stream through a saturator (4) containing the toluene, and then mixing with air and He before reaching the catalyst. The flow rate of the reactant mixture was 20 cm^3min^{-1} with a resulting space velocity (GHSV) of 7.6 × $10^{-3}mol_{VOC}h^{-1}$ g_{cat}^{-1}. The effluent gases were analysed on-line by a gas chromatograph, equipped with a packed column with 10% FFAP on ChromosorbW and FID detector, and by a quadrupole mass spectrometer (7) (VG quadropoles). The carbon balance was always higher than 95%.

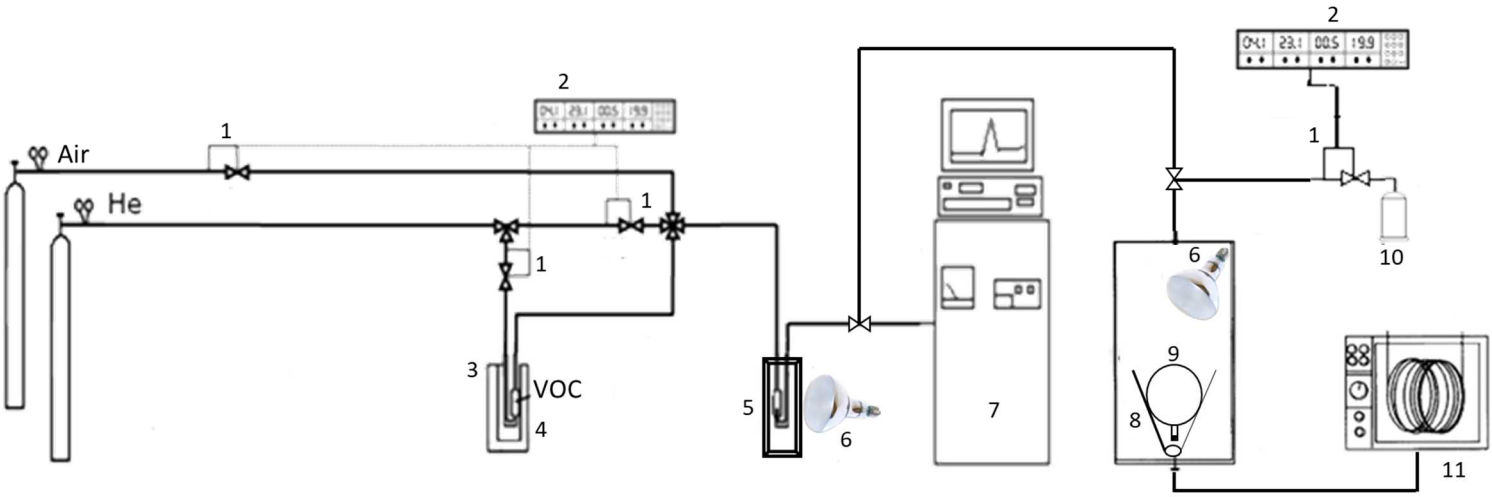

Figure S1. Scheme of the used experimental set-up: (1) Gas flow controllers; 2) Tylan gas flow controller unit; 3) Thermostat; 4) VOC saturator; 5) Heated flow reactor; 6) Solar lamps; 7) GC-MS; 8) Heating bands; 9) Pyrex batch photoreactor; 10) Water bubbler; 11) GC.

The obtained CO_2 was flowed in a second cylindrical Pyrex batch photoreactor (9), using an identical solar lamp (6) employed also for the toluene removal. Before the measurements, the catalysts were left overnight under He flow (20 cc/min) and UV irradiation (using a 100W mercury lamp, Black-Ray B-100A, 365 nm) in order to remove the possible contaminants and/or the carbonaceous species present in the sample surface. Afterwards, a mixture of water vapour- He flow (25 cm^3/min) was flowed inside the reactor and several portions of the gas in output were examined by gas-chromatography (GC) to monitor the efficacy of the cleaning process and the potential existence of residual carbonaceous contamination. The H_2O vapours (10) were mixed with the CO_2 and flowed inside the photoreactor to attain the saturation of the sample surface with the reactant gases. By means of gas flow controllers ((1) and (2)) the flow rate of the mixture CO_2/H_2O was set in order to obtain a molar ratio of 15. In this way, on the surface of the catalysts, the CO_2 adsorption/reduction was favoured, inhibiting the competitive water splitting reaction [3,4].

The catalyst (200 mg, 80–140 mesh) was contextually heated (at 120°C) by means of heating bands

(8) and irradiated for 5h. The obtained products were analysed with the GC Agilent 6890N equipped with a TCD detector and a HP-PLOT Q column (for the CO and the CH_4 detection) and with the Trace GC instrument with a FID detector (Porapak Q column,) to identify the potential formation of organic products.

- **Textural and optical properties of the examined samples**

Table S1 BET surface areas and optical bandgaps (Eg) of the examined samples.

Samples	**S_{BET} ($m^2 g^{-1}$)**	**E_g (eV)**
Mn_3O_4	87	3.3
ZrO_2	25	3.0
MnZr5	85	3.3
CeO_2	60	2.9
Brookite TiO_2	80	3.2
TiCe3	68	3.4
CuO/TiCe3	67	3.6
Cu_2O/TiCe3	70	3.2
CuO_x/TiCe3	74	3.0

- **Crystalline structure and morphology of the MnO_x-based samples**

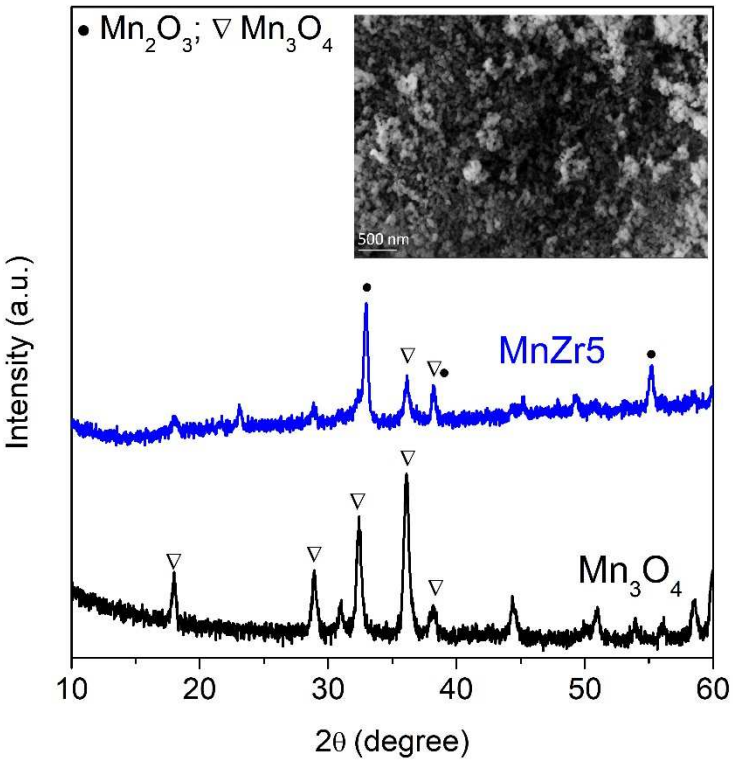

Fig. S2 XRD patterns of the MnO_x-based samples. In the inset the SEM image of the MnZr5 sample.

- **Comparison of the amounts of solar fuels formation with the CuO_x/TiCe3 catalyst between the solar photocatalytic, thermocatalytic and the solar photo-thermal co-catalytic tests.**

Table S2 Comparison of the different catalytic approaches using the CuO_x/TiCe3 sample for the CO_2 conversion.

	CO formation ($\mu mol/g_{cat} \cdot h$)	CH_4 formation ($\mu mol/g_{cat} \cdot h$)
Photothermo-catalysis*	12.23 (80°C) 17.6 (120°C) 25.2 (180°C) 36.2 (260°C) 46.3 (340°C)	5.0 (80°C) 7.9 (120°C) 9.9 (180°C) 15.2 (260°C) 18.6 (340°C)
Thermocatalysis	/ (80°C) / (120°C) 6.3 (180°C) 25.1 (260°C) 101.9 (340°C)	/ (80°C) / (120°C) 2.5 (180°C) 12.6 (260°C) 31.6 (340°C)
Photocatalysis*	4.9 (30°C)	1.6 (30°C)

* after 5h of simulated solar irradiation

- **Structural and morphological properties of the TiCe3-based materials**

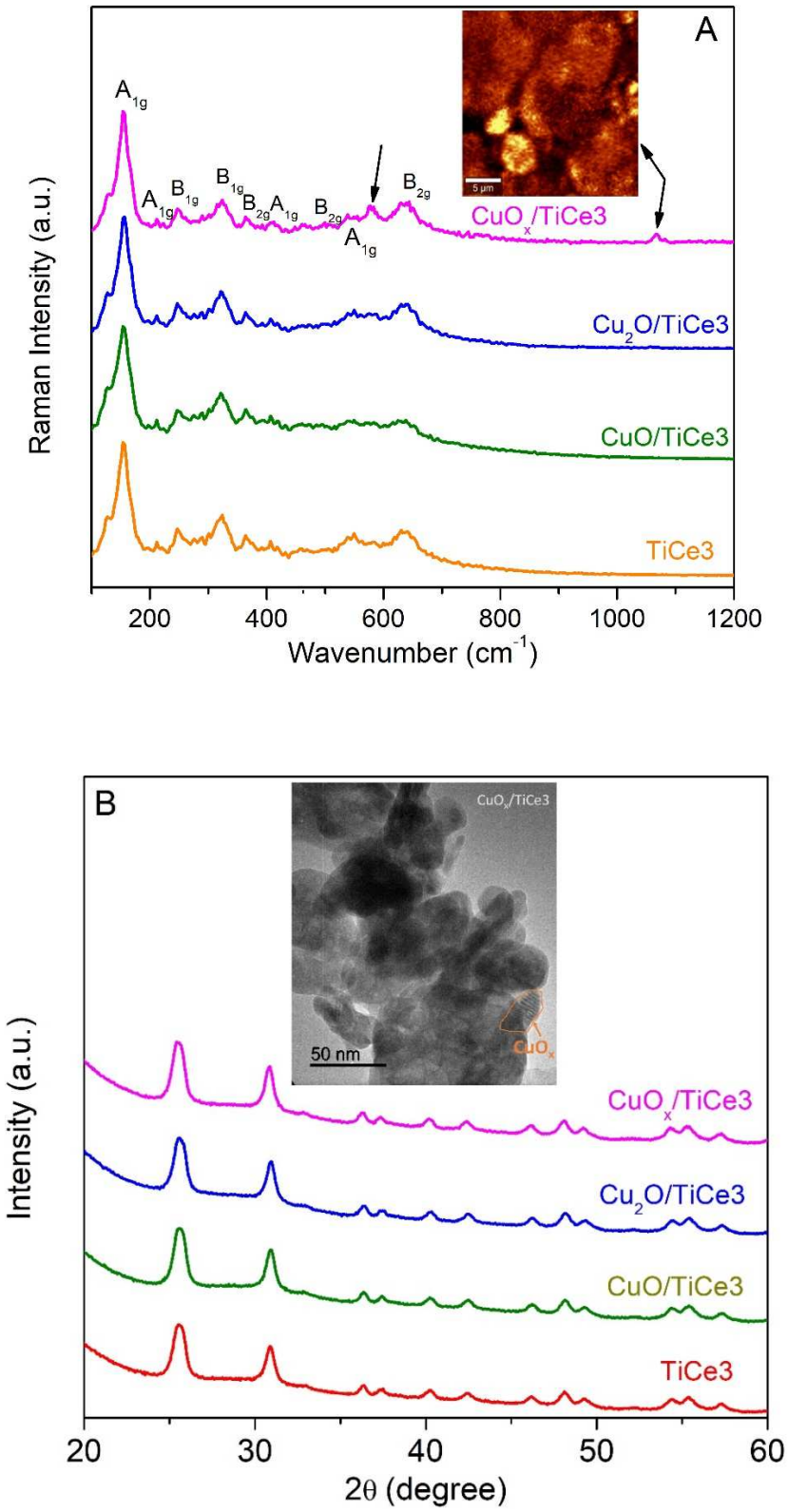

Fig. S3 (A) Raman spectra and (B) XRD patterns of the examined samples. In the inset of Fig. S3A the Raman confocal map, where the yellow areas are the regions of the sample where the peak at 1067 cm^{-1} is more intense. In the inset of the fig. S3B the TEM image of the CuO_x/TiCe3 sample.

- **XPS analysis: Ti 2p and Cu 2p region**

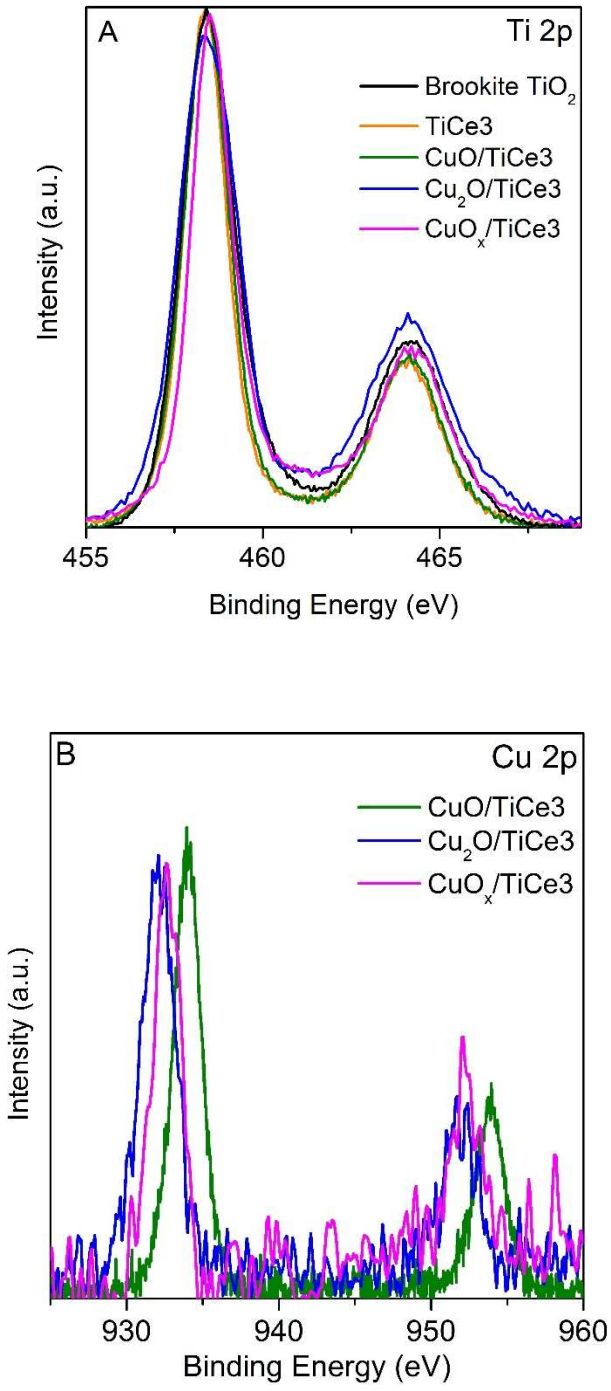

Fig. S4 (A) Al Kα excited XPS of the examined samples measured in the Ti 2p binding energy region (B) Al Kα excited XPS of the examined samples measured in the Cu 2p binding energy region.

- **XPS analysis: Surface atomic concentration analyses**

Table S3 XPS atomic concentration analyses of the best copper-based TiCe3 samples.

	(Ce/Ti)·100	Nominal (Ce/Ti)·100	(Cu/Ti)·100	Nominal (Cu/Ti)·100
Cu_2O/TiCe3	4.0	1.4	4.0	0.58
Cu_2O/TiCe3 after test	1.5	1.4	5.0	0.58
CuO_x/TiCe3	2.7	1.4	2.7	0.66
CuO_x/TiCe3 after test	2.3	1.4	11.2	0.66

- **Optical properties of the TiCe3-based samples**

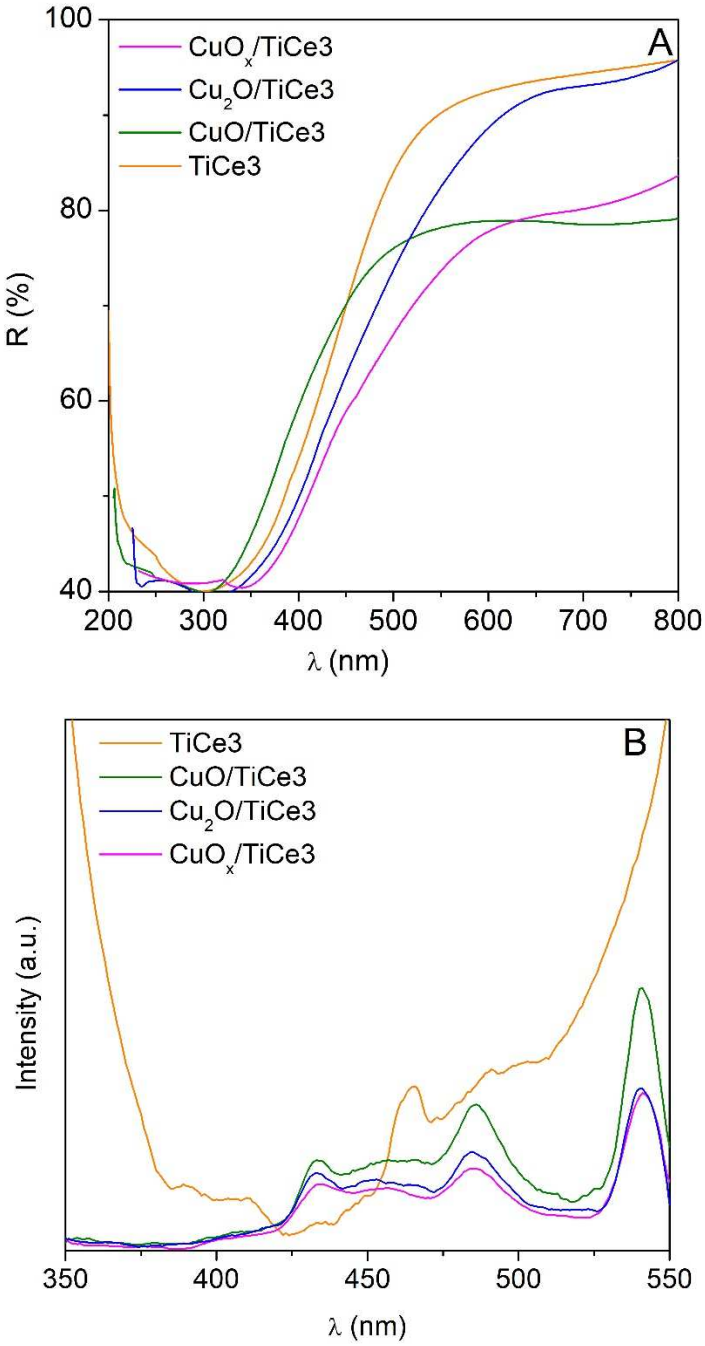

Fig. S5 (A) UV-DRS spectra and (B) Photoluminescence spectra ($\lambda_{excitation}$=300 nm) of the examined samples.

- **Apparent activation energy of the solar photo-thermo co-catalytic CO_2 reduction with the CuO_x/TiCe3 catalyst**

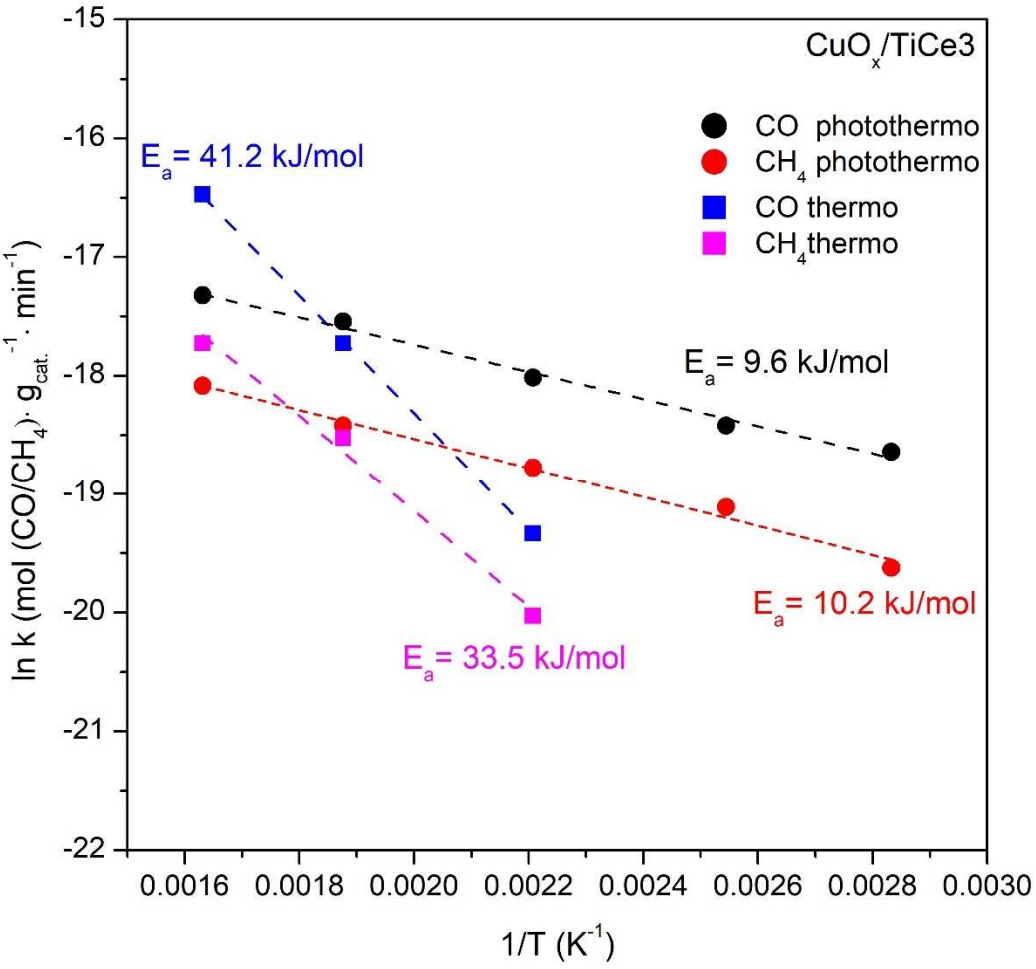

Fig. S6 Apparent activation energy calculated with the Arrhenius equation, for the CO and the CH_4 formation on CuO_x/TiCe3 sample on the basis of the catalytic approaches. No solar fuels formation was detected in the themocatalytic tests at 80°C (1/T = 0.0028 K^{-1}) and 120°C (1/T = 0.0026 K^{-1}).

- **FTIR spectra before and after the solar photo-thermo co-catalytic CO_2 conversion**

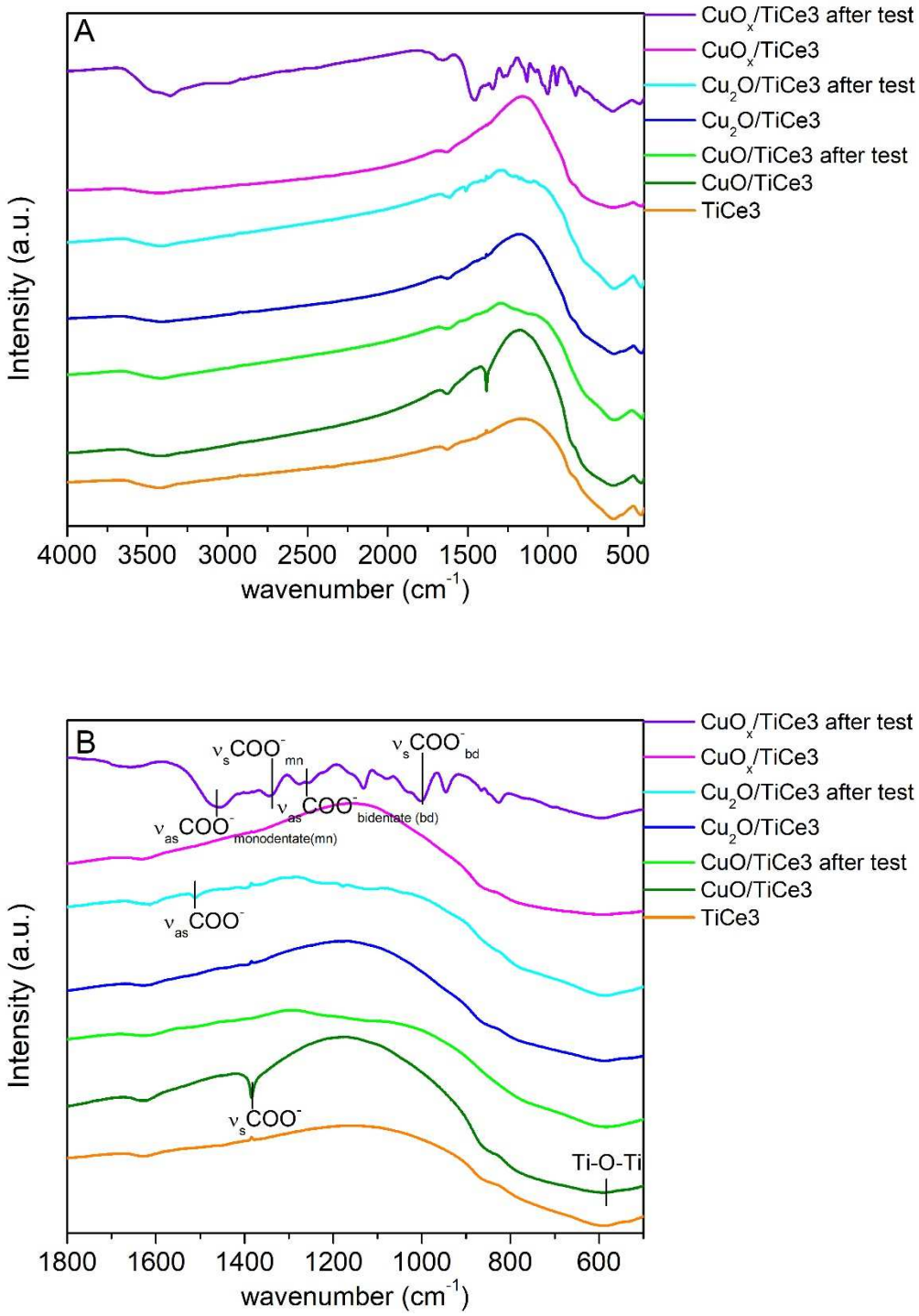

Fig. S7 (A) Comparison of the FTIR spectra before and after the photo-thermo co-catalytic CO_2 reduction; (B) Focus on the "carbonates" region.

- **Catalytic stability of the CuO_x/TiCe3 sample in the the solar photo-thermo co-catalytic CO_2 conversion**

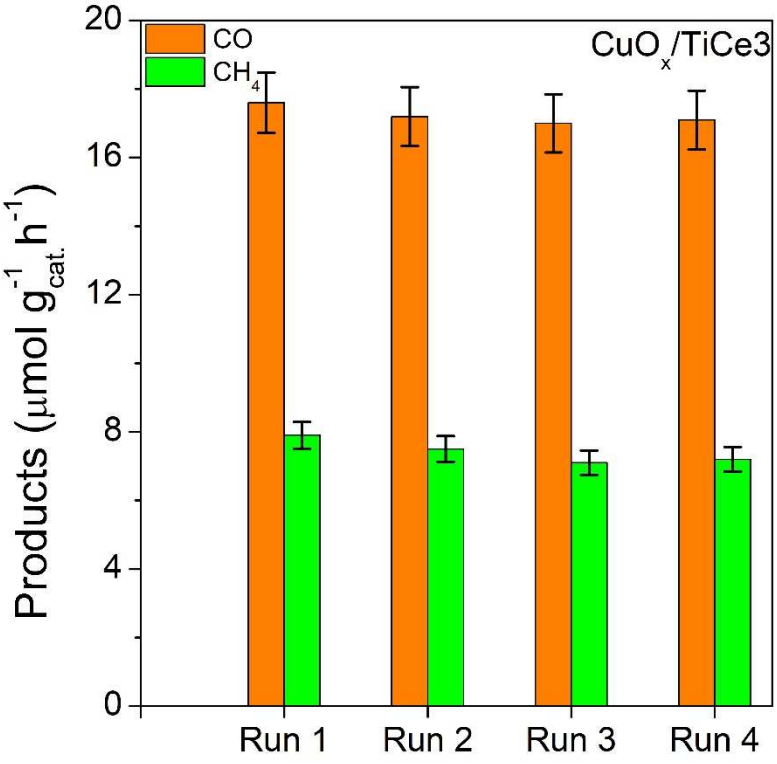

Fig. S8 Catalytic stability after 4 consecutive runs of the solar photo-thermo co-catalytic CO_2 conversion on CuO_x/TiCe3 sample.

References:

[1] D. Briggs, J. T. Grant, Surface Analysis by Auger and X-Ray Photoelectron Spectroscopy, 2003 IMP, Chichester, UK.

[2] A. Gulino, Anal. Bioanal. Chem. 2013, 405, 1479–1495.

[3] R. Fiorenza, M. Bellardita, S.A. Balsamo, L. Spitaleri, A. Gulino, M. Condorelli, L. D'Urso, S. Scirè, L. Palmisano, Chem. Eng. J. 428 (2022).

[4] E. Karamian, S. Sharifnia, J. CO_2 Util. 16 (2016) 194–203.